Electronic Supplementary Material (ESI) for Physical Chemistry Chemical Physics.

Photoinduced absorption spectroscopy (PIAS) study of water and chloride oxidation by a WO_3 photoanode in acidic solution

James Johnston*, Christopher O'Rourke, and Andrew Mills

Electronic Supplementary Information (ESI)

School of Chemistry and Chemical Engineering, Queens University Belfast, Stranmillis Road, Belfast, BT9 5AG, UK

key words: photocatalysis; semiconductor; mechanism; water oxidation; chloride oxidation

Contents

S1 – Schematic of electrochemical reaction cell

The reaction cell used for all photoelectrochemical measurements (except for the PIAS and IPCE experiments) is shown in **Figure S1**. The cell is made from PTFE (polytetrafluoroethylene), and features an opening at the bottom, sealed using the photoanode, a Pt coil as the counter electrode, an opening to accommodate a Ag/AgCl reference electrode, and an inlet and outlet for purging the electrolyte, which was 10 mL of either 1M $HClO_4$ (for water oxidation) or 1 M $HClO_4$ + 3.5 M NaCl for chloride oxidation. The photoanode was usually irradiated through the back of the photoanode using a 365 nm LED (40 mW cm^{-2}).

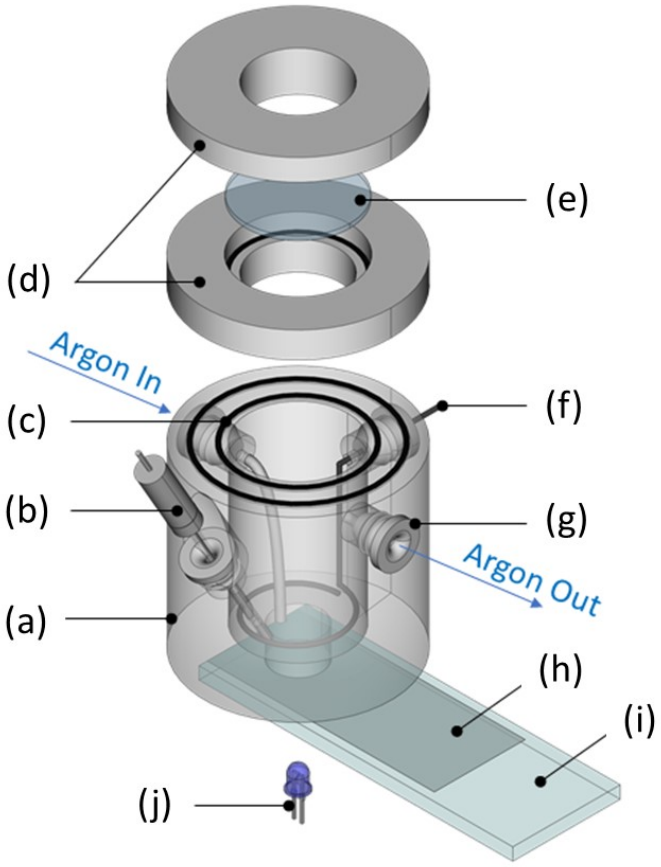

Figure S1 - Exploded-view schematic of the PTFE vessel used for photoelectrochemical experiments: (a) PTFE main body, (b) Ag/AgCl reference electrode, (c) O-rings, (d) PTFE lid, (e) quartz window, (f) Pt-coil counter electrode, (g) Suba-Seals®, (h) WO_3 film photoanode, (i) conductive glass, (j) 365 nm LED.

S2 – Determination of the faradaic efficiency for O_2 generation, f_{O2}

A schematic illustration of the setup used to determine f_{O2} is shown in **Figure S2.1(a)**. In this setup, a mass flow controller (Aalborg, Orangeburg, USA) was used to regulate a constant 0.1 mL s^{-1} flow of argon through the PTFE vessel. Any O_2 produced in the photo-electrochemical reaction cell (see **Figure S1**) was carried through to the 3D printed holder (see **Figure S2.1(b)**), containing a fluorescence-based oxygen sensor, O_2xyDot™ (O_2xyDot®, OxySense, Devens, USA), which was maintained at 25 °C using a circulating water bath (RCB20-PLUS, Hoefer, Holliston, USA). The change in lifetime of the sensor was measured using a NEOFOX-GT probe (Ocean Insight, Orlando, USA), from which a value for the % O_2 in the argon carrier gas stream was determined, *via* the Stern-Volmer equation.

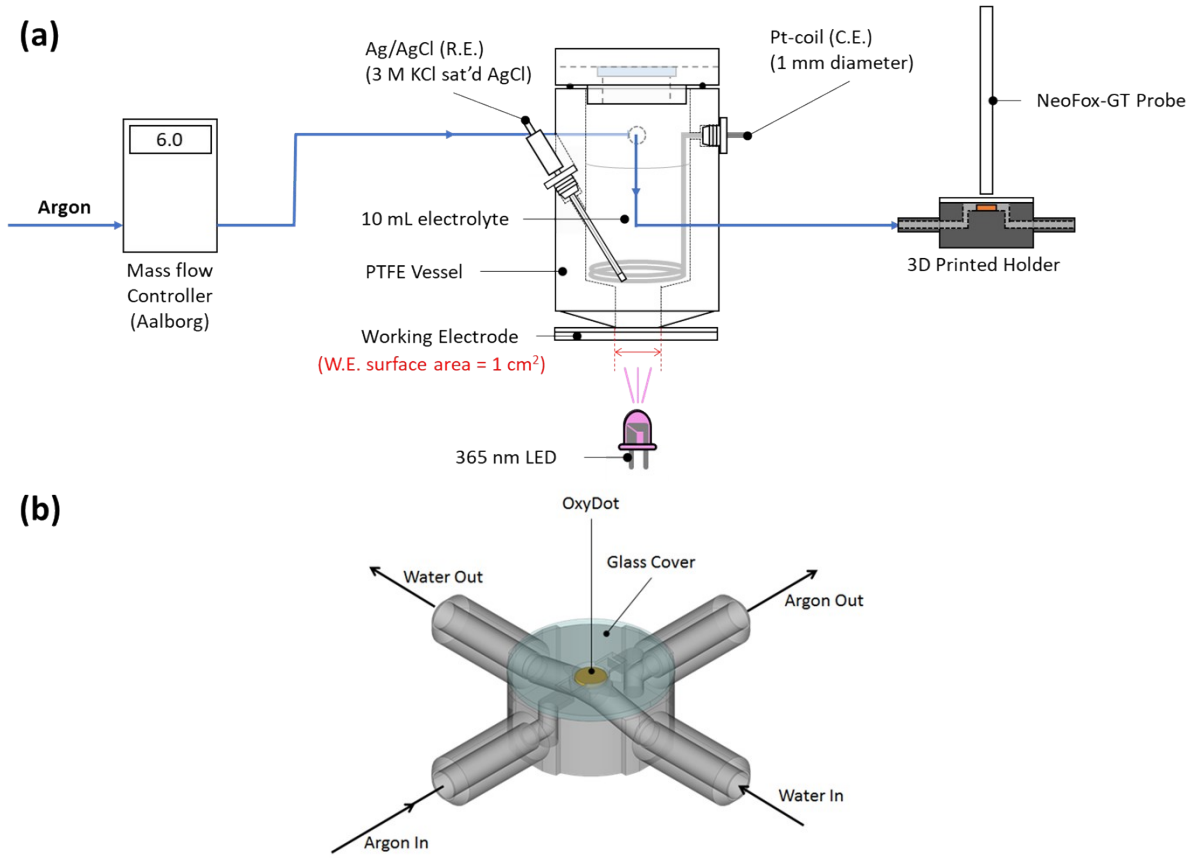

Figure S2.1 – (a) Schematic of setup used for the determination of f_{O2}. Argon is passed through the PTFE vessel at 0.1 mL s^{-1}, carrying any O_2 produced in the PTFE vessel through to the 3D printed thermally regulated holder containing a fluorescence-based oxygen sensor, O_2xyDot™. The change in lifetime of the sensor, measured using a NeoFox-GT Probe, allows the determination of the % O_2 in the argon carrier gas stream. **(b)** Schematic of the custom-made, 3D-printed thermally regulated O_2 detector cell. Water was passed through the holder using a thermostatted circulating bath set at 25°C.

In this work, the WO_3 photoanode was placed in the electrochemical reactor (see **Figure S1**), which contained 10 mL of 1 M $HClO_4$, and irradiated with 40 mW cm^{-2} 365 nm UVA, while poised at the potential which would generate a steady current density of 0.1 mA cm^{-2} (ca. 1.0 V vs Ag/AgCl). The

reaction cell was continually flushed with Ar (0.1 mL s^{-1}), and the gas outlet was monitored by the O_2 sensor, which yielded a % O_2 vs irradiation time profile illustrated in **Figure S2.2**, from which a plateau value of 0.0066 % (the average % O_2 value between t=100 min and t =120 min) was determined. The value of f_{O2} was then calculated using the following expression,

$$f_{O2} = \frac{\text{actual \% O}_2}{\text{theoretical \% O}_2} \#(S1)$$

where the 'actual %O_2' was taken as 0.0066 %, and the value of the theoretical O_2 was calculated using the following equation

$$\text{theoretical \% O}_2 = 100 \text{ x} \frac{24200i}{\text{F}nr} \#(S2)$$

where *i* is the current (1 x10^{-4} A), F is Faradays constant (96485 C mol^{-1}), *n* is the number of electrons transferred in the oxidation of H_2O to O_2 (4 electrons), *r* is the flow rate of the carrier gas (0.1 mL s^{-1}), and 24200 is the volume, in mL, occupied by 1 mol of gas at room temperature and pressure. The value for the theoretical % O_2 was calculated to be 0.0063 %, and so, from equation (S1) it follows that f_{O2} =0.0066/0.0063 ≈ unity.

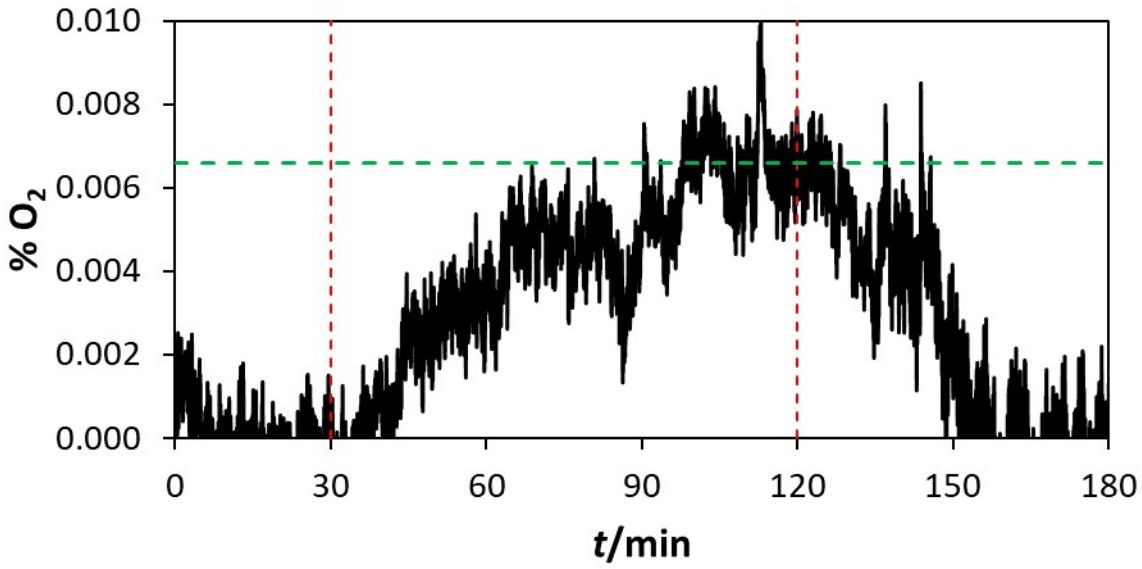

Figure S2.2 - The change in % O_2 with *t*, recorded for the WO_3 photoanode in 1 M $HClO_4$, under 40 mW cm^{-2} 365 nm irradiation. The red dashed lines indicate the initiation and termination of applied potential (set to maintain a constant current of 0.1 mA, *ca.* 1 V vs Ag/AgCl), and the green dashed line indicates the actual steady state yield in % O_2, 0.0066 %, calculated as the average % O_2 value between *t* =100 min and *t* = 120 min.

S3 – Determination of the faradaic efficiency for Cl_2 generation, f_{Cl2}

To determine the value of f_{Cl2} for the WO_3 photoanode in the 1 M $HClO_4$ + 3.5 M NaCl electrolyte solution under UV irradiation, a KI trap was placed in line after the electrochemical cell, comprising of a Drechsel bottle containing a 100 mL aqueous solution of KI (0.36 M), potassium hydrogen phthalate (0.049 M), and NaOH (0.025 M).[1] The setup used is illustrated in **Figure S3.1**.

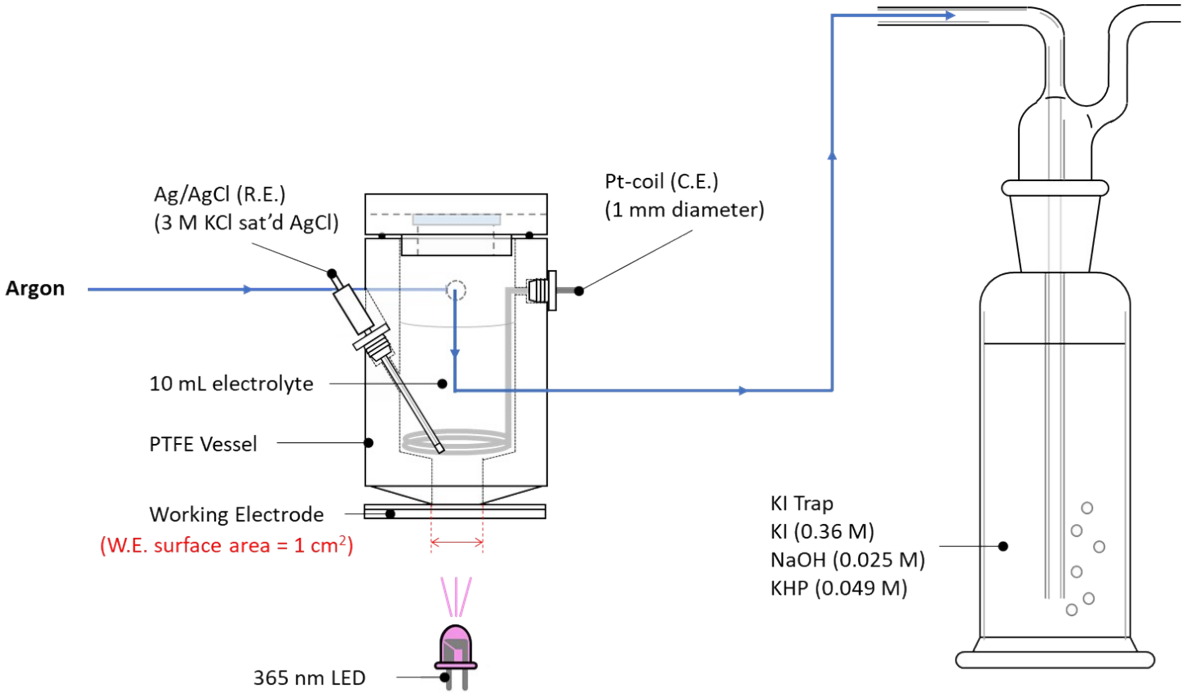

Figure S3.1 - Schematic of the setup used for the determination of f_{Cl2}. Argon is passed through the PTFE vessel to a KI trap containing a 100 mL solution comprising of potassium iodide (0.36 M), sodium hydroxide (0.025 M), and potassium hydrogen phthalate (0.049 M).[1] Any Cl_2 flushed over to the KI trap produces I_3^-, the absorbance of which can be monitored by UV-vis spectroscopy, allowing quantification of the amount of Cl_2 produced.

The WO_3 photoanode was irradiated (40 mW cm^{-2}, 365 nm) and poised at 1 V vs Ag/AgCl for 30 minutes, while the sealed PTFE electrochemical reaction cell was continually purged with Ar, flushing any photogenerated Cl_2 from the reaction solution in the photoelectrochemical reactor through to the KI trap solution, where it generated I_3^-, which absorbs strongly at 353 nm (ε_{353}=26400 mol^{-1} cm^{-1}).[1, 2] The reaction vessel was continually flushed with Ar for 2 hours after the applied potential and irradiation had ceased, so that all the photogenerated Cl_2 was captured by the trap, and then the UV-vis absorbance of the trap solution was measured using a 1 mm quartz cuvette and yielded the absorbance spectrum (solid line) shown in **Figure S3.2(b)**.

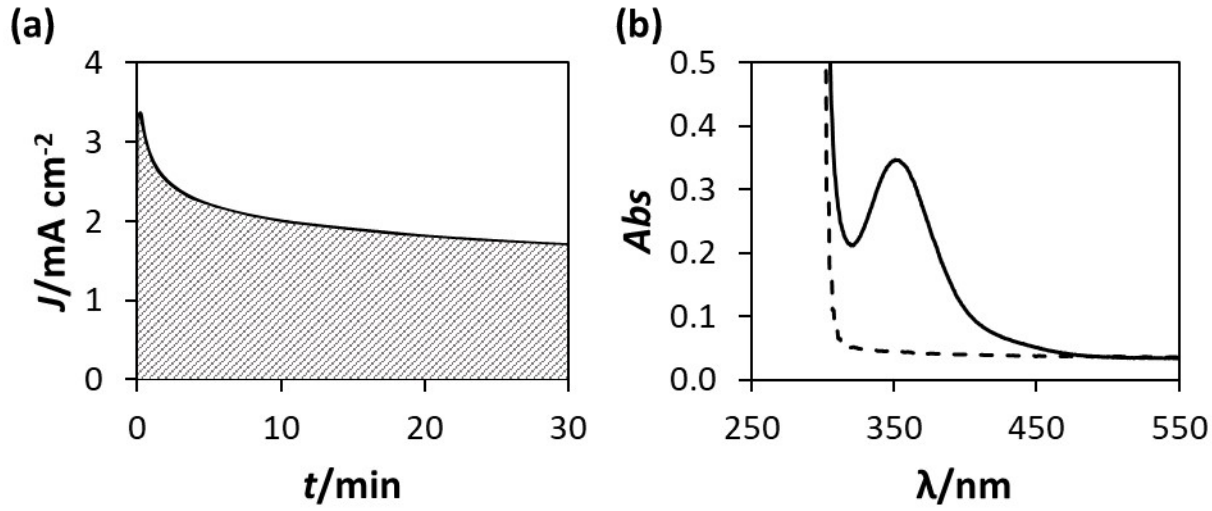

Figure S3.2 - **(a)** The chronoamperometry profile showing the variation in current density (*J*) with time (*t*), with the shaded area representing the total charge transferred, *Q*, and; **(b)** the UV-vis absorbance spectrum of the KI trap solution before (dashed line) and after (solid line) photogenerated Cl_2 had been flushed into the trap and ΔAbs_{353} stopped increasing, recorded in a 1 mm quartz cuvette.

The absorbance due to a chemical species, *Abs*, is related to the concentration, c, of the species, according to the Beer-Lambert law,

$$Abs = \varepsilon c l \quad \#(S3)$$

where ε is the molar absorption coefficient of the species, and l is the path length the light passes through. The absorbance at 353 nm of the KI trap solution before the chloride oxidation procedure was 0.043, and after the procedure was 0.346, thus the absorbance due to I_3^- generation was (0.346-0.043) = 0.303. This absorbance was divided by the molar absorption coefficient for I_3^- at 353 nm (26400 L mol^{-1} cm^{-1}),[1, 2] and the path length (0.1 cm) to determine $[I_3^-]$ in the KI trap to be 0.303/(26400x0.1)= 1.15×10^{-4} M.

Since the trapping solution was 100 mL in volume, this means the amount of I_3^- generated was 1.15×10^{-5} mol. Stoichiometrically, each molecule of I_3^- is generated by one Cl_2 molecule, so the actual yield of Cl_2 was also 1.15×10^{-5} mol.

f_{Cl2} was determined using the expression

$$f_{Cl2} = \frac{\text{actual yield of } Cl_2}{\text{theoretical yield of } Cl_2} \quad \#(S4)$$

where the theoretical yield of Cl_2 was calculated using

$$\text{theoretical yield of } Cl_2 = \frac{Q}{nF} \quad \#(S5)$$

where Q is the total charge transferred (equal to the shaded area under the chronoamperometry trace in Figure 3.2(a), multiplied by the exposed electrode surface area (ca. 1 cm^2), which works out as 3.58 C), F is Faraday's constant (96485 C mol^{-1}) and n (=2) is the number of electrons transferred in the oxidation of chloride ions to generate 1 Cl_2 molecule ($2Cl^- \rightarrow Cl_2 + 2e^-$).

Thus, the theoretical yield of Cl_2 was determined to be 3.58/(2x96485) = 1.86×10^{-5} mol, and so f_{Cl2} was determined to be $1.15 \times 10^{-5} / 1.86 \times 10^{-5}$ = 0.62. Although this is a high yield, it is far from unity, thus indicating that either there was an oxidation product, or products, generated other than Cl_2, or that a significant fraction of the generated Cl_2 did not make it to the trap solution, most likely by reacting with components of the cell, such as plastic tubing, the reactor cell wall or the Suba-Seals®.

S4 - Schematic of PIAS/IPCE cell

For PIAS and IPCE experiments, the 3D printed (polylactic acid) PIAS cell illustrated below (**Figure S4**) was used to host the reaction components: the electrolyte (*ca.* 10 mL), working electrode (WO_3), counter electrode (Pt coil) and reference electrode (Ag/AgCl). There were quartz windows on either side of the cell, to allow transmission of excitation electromagnetic radiation, λ_{excit} (and in the case of PIAS the monitoring beam radiation, usually set at 500 nm), through the cell.

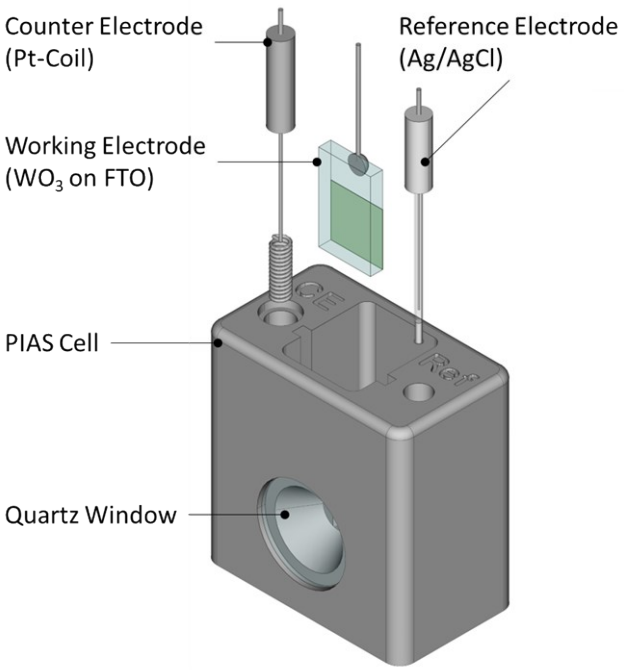

Figure S4 – Exploded view of the PIAS cell, showing how the 3 electrodes are inserted into the 3D printed cell. The working electrode is held in place between 2 quartz windows, allowing the transmission of the excitation radiation and (for PIAS) the monitoring beam.

S5 – Incident photon to current efficiency (IPCE) measurements

A schematic of the setup used to determine incident photon to current efficiencies is illustrated in **Figure S5.1**. In this system, a 1 kW Xe-Arc lamp (KiloArc™, Optical Building Blocks Corporation, Pemberton, USA) delivered the excitation light, the wavelength of which, λ_{excit}, was controlled using a monochromator (Optical Building Blocks Corporation, Pemberton, USA).

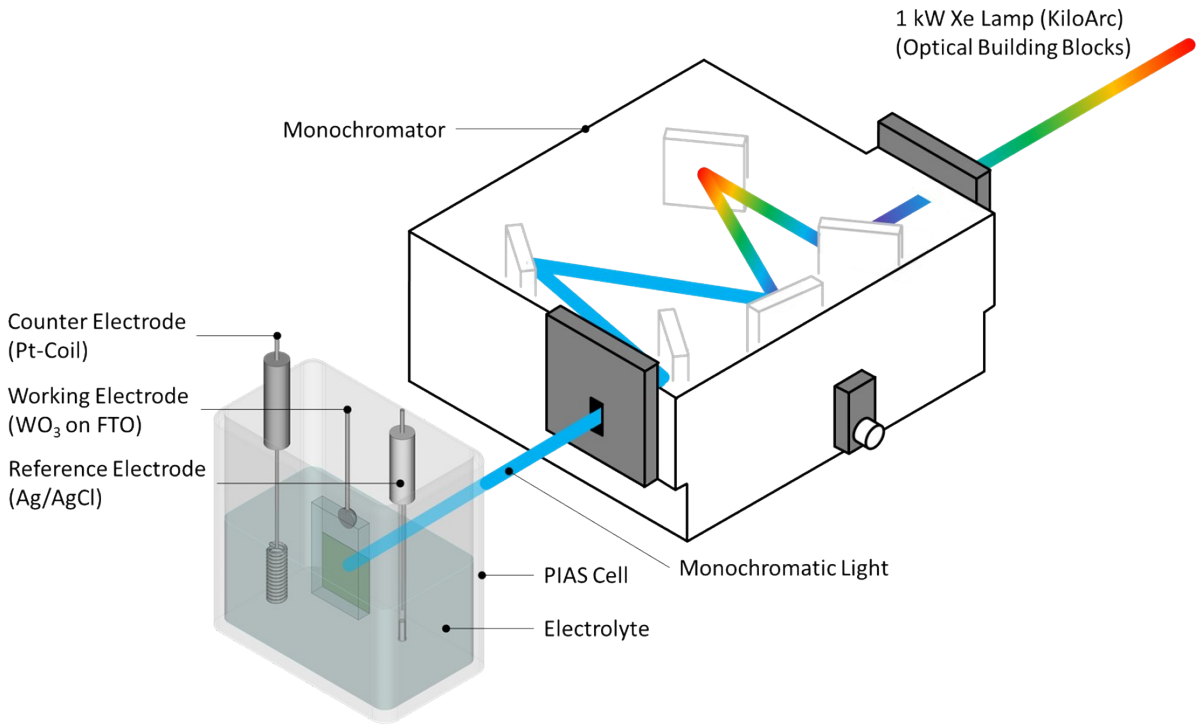

Figure S5.1 - Schematic of the IPCE setup. Monochromatic light from 300 nm to 500 nm in 10 nm steps was achieved using a 1 kW Xe lamp connected to a monochromator. The monochromatic light was directed through the window of a PIAS cell, illuminating a 0.636 cm^2 area of the WO_3 working electrode.

To calculate the IPCE value at each value of λ_{excit} it is necessary to determine the photon flux delivered to the photoanode, and the photocurrent generated in response to this illumination. To determine the former, the irradiance vs wavelength profile of each of the apparently monochromatic light beams, set at λ_{excit}, delivered by the 1 kW Xe-Arc lamp/monochromator, incident to the photoanode in IPCE photocurrent measurements were recorded using a calibrated spectroradiometer (OL 756, Gooch and Housego, Ilminster, UK), at 10 nm increments from 300 – 500 nm (controlled by a monochromator). The irradiance vs wavelength profiles recorded for each selected value of λ_{excit}, and the photon flux calculated from this data for each selected value of λ_{excit} are shown in **Figure S5.2**.

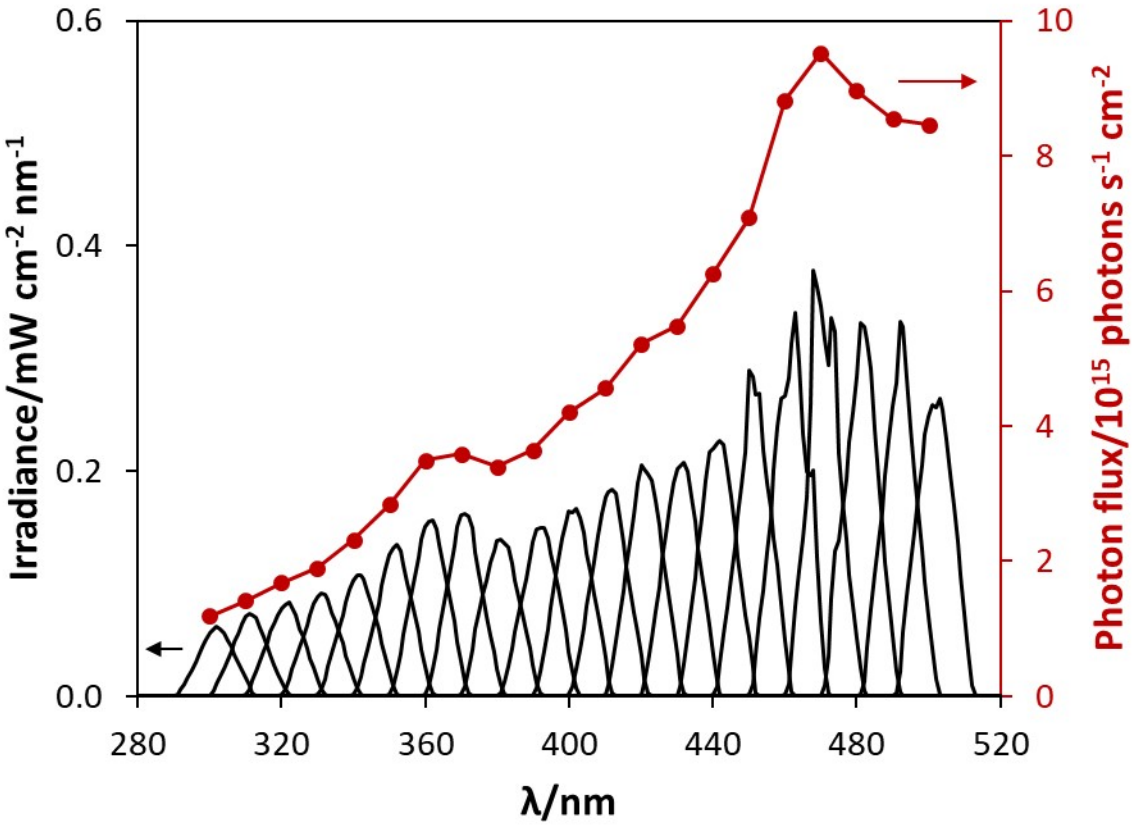

Figure S5.2 - The irradiance (ρ) of the Xe-Arc lamp, measured at different λ_{excit} values, which range from 300 nm to 500 nm (every 10 nm). The black lines show the irradiance profiles, and the red data points show the sum photon flux output for each irradiance profile at each emission maximum, λ_{excit}.

Photon flux was calculated from the irradiance measurements made at each λ_{excit} value using the following equation

$$\text{photon flux (photons s}^{-1}\text{cm}^{-2}) = \frac{\rho\ (\text{W cm}^{-2})\ \text{x}\ \lambda(\text{m})}{\text{h(J s) x c(m s}^{-1})} \#(S6)$$

where h is Planck's constant (6.63×10^{-34} J s), *c* is the speed of light (3.0×10^{8} m s^{-1}), and λ is the excitation wavelength (m). To illustrate how photon flux was calculated for each irradiance spectrum recorded for a set value of λ_{excit}, we take here as an example the irradiance profile measured at λ_{excit} 300 nm, which is shown in **Figure S5.2** and magnified in **Figure S5.3**. **Figure S5.3** shows that the spectrum for the 300 nm λ_{excit} peak is made up of individual irradiance data points, measured for every nm in the studied range, i.e. ρ_{λ} values, where λ ranges from 280 to 520 nm (Figure S5.3 shows ρ_{λ} values between 280 to 325 nm only, for illustrative purposes), but with a peak maximum at λ_{excit}, which in this case is 300 nm.

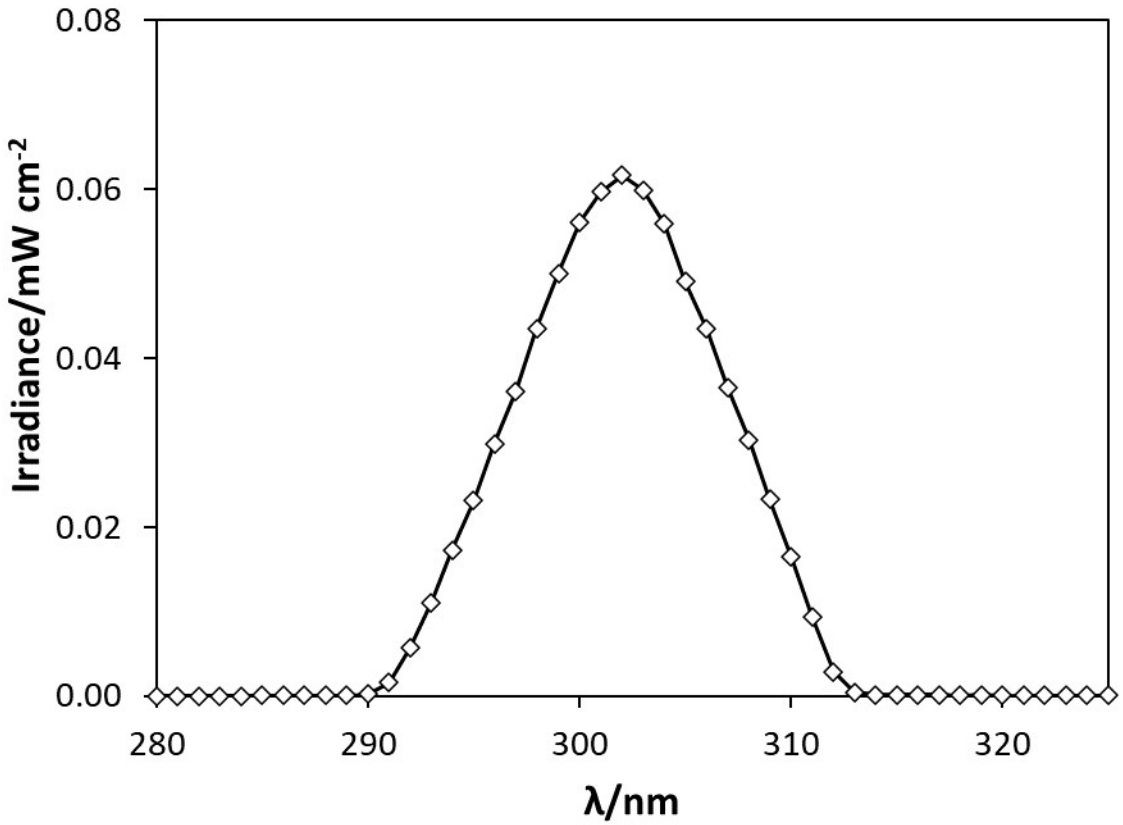

Figure S5.3 – The irradiance profile, shown between 280 nm – 325 nm, delivered by the 1 kW Xe Arc lamp when the monochromator was used to select λ_{excit} to be 300 nm. The diamond data points show the measured irradiance values at each wavelength, ρ_{λ}, that comprises the beam of radiation used to excite the photoanode that emerges from the 1KW/monochromator system illustrated in Figure S5.1, when the monochromator is set at λ_{excit} = 300 nm

For each ρ_{λ} value, the corresponding photon flux was calculated according to equation (S6). For example, in **Figure S5.3**, the irradiance a 291 nm, ρ_{291}, was $1.6x10^{-3}$ mW cm^{-2}, and so

$$\text{photon flux291} = \frac{1.6x10^{-6} \text{ x } 291}{6.63x10^{-34} \text{ x } 3x10^{8}} = 2.35x1012 \text{ photons s - 1 cm - 2 } \#(S7)$$

In the same manner, photon flux was calculated for each ρ_{λ} value at each value of λ (from 280 nm to 520 nm), that forms the beam of radiation used to excite the photoanode that emerges from the 1 kW/monochromator system illustrated in **Figure S5.1**, when the monochromator is set at λ_{excit} = 300 nm. These values are then summed, to determine the total photon flux delivered by the 300 nm, λ_{excit}, beam, which in the case of the λ_{excit} emission peak illustrated in Figure S5.3 = $18x10^{15}$ photons s^{-1} cm^{-2}, as shown by the appropriate red coloured data point in **Figure S5.2**. This same method was applied to determine the photon flux delivered by the 310, 320, 330 etc. nm beams of irradiation used to excite the photoanode that emerges from the 1 kW/monochromator system illustrated in **Figure S5.1**,

when the monochromator is set at λ_{excit} = 310, 320, 330 etc. nm, thereby generating the data necessary to construct the photon flux vs λ_{excit} data points shown in red in **Figure S5.2**.

To determine IPCE, the photocurrent generated under these same irradiation conditions was measured using the setup illustrated in **Figure S5.1**. Thus, the photoanode was exposed to a beam of radiation from the 1 kW/monochromator system illustrated in **Figure S5.1**, when the monochromator is set at λ_{excit}, and the photocurrent measured. Photocurrent density (J) was determined by dividing the photocurrent by the irradiated photoanode surface area (*ca.* 0.636 cm^2). In this work the excitation beam of radiation was mechanically chopped (5 s on 5 s of) 5 times, and the average "light on" photocurrent density ($J_{average}$) recorded, before the value of λ_{excit} was altered by 10 nm and the process repeated as λ_{excit} was varied from 300 to 480 nm. In this work the radiation was used to excite a WO_3 photoanode, held at 1.3 V vs. Ag/AgCl, in 1 M $HClO_4$, and in 1 M $HClO_4$ + 3.5 M NaCl. The average photocurrent densities for each value of λ_{excit} were calculated and are shown in **Figure S5.4**, for both electrolyte solutions.

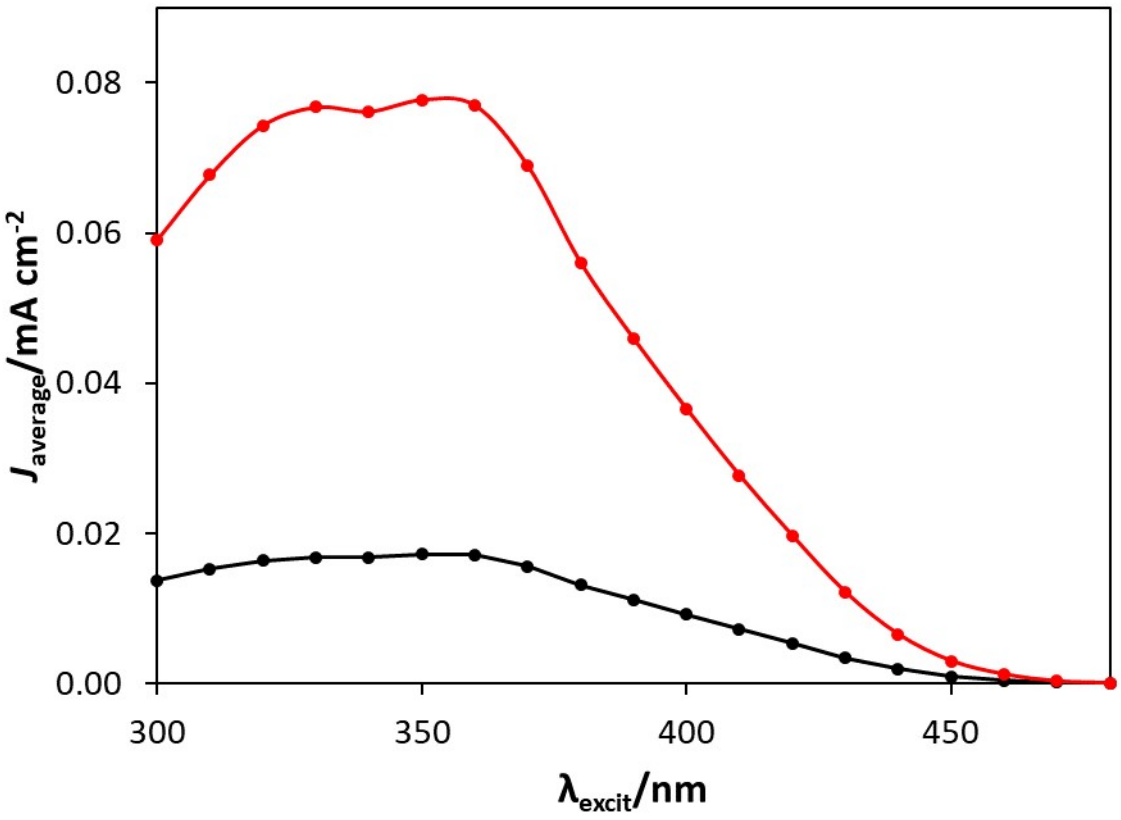

Figure S5.4 - The average photocurrent densities generated upon irradiation of the WO_3 photoanode, poised at 1.3 V vs Ag/AgCl, in 1 M $HClO_4$ (black) and 1 M $HClO_4$ + 3.5 M NaCl (red), using different values of excitation wavelength, λ_{excit}. This data was combined with the photon flux for each λ_{excit} value, to generate IPCE values, using an equation of the form of equation (S7).

IPCE values were calculated using the following expression,[3]

$$\text{IPCE} = 100 * \frac{\text{photocurrent density (electrons s}^{-1}\text{cm}^{-2})}{\text{photon flux (photons s}^{-1}\text{cm}^{-2})} \#(S8)$$

As an example calculation, for the WO_3 photoanode in 1 M $HClO_4$, at λ_{excit} = 300 nm the average photocurrent density was 1.375×10^{-5} A cm^{-2} (see **Figure S5.4**), which was divided by the charge of one electron (1.6×10^{-19} C) to express the photocurrent density as 8.59×10^{13} electrons s^{-1} cm^{-2}. Then, using equation (S8), and the value of photon flux for 300 nm emission determined previously (1.18×10^{15} photons s^{-1} cm^{-2}, see **Figure S5.2**) the IPCE for the WO_3 photoanode (held at 1.3 V (vs Ag/AgCl), in 1 M $HClO_4$) under 300 nm irradiation was determined as

$$\text{IPCE (1 M HClO}_4\text{, 300 nm)} = 100 \text{ x } \frac{8.59\text{x}1013}{1.18\text{x}1015} = 7.28\ \% \#(S9)$$

The full IPCE spectrum obtained for the WO_3 photoanode, poised at 1.3 V vs Ag/AgCl, in 1 M $HClO_4$, is shown in black, in **Figure S5.5**, and **Figure 4** in the main text.

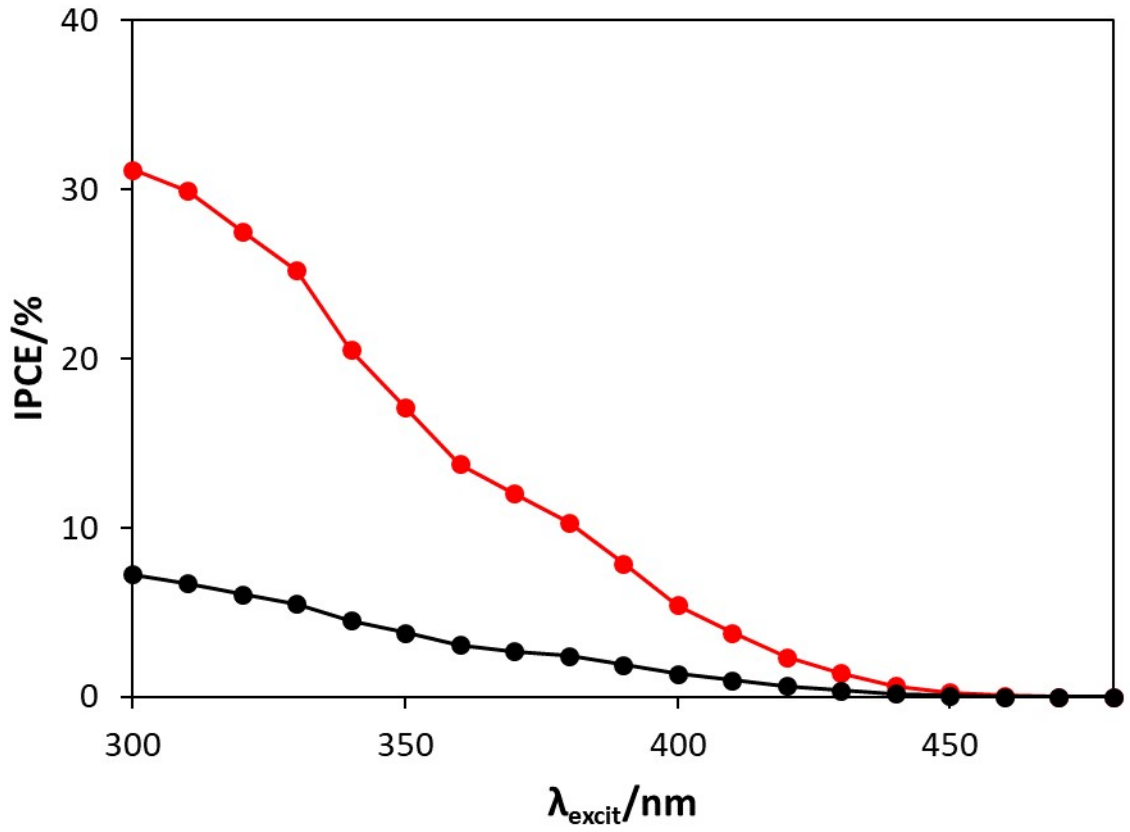

Figure S5.5 - The IPCE spectra between 300 to 480 nm for the WO_3 photoanode in 1 M $HClO_4$ (black) and 1 M $HClO_4$ + 3.5 M NaCl (red), irradiated by a 1 kW Xe-Arc lamp.

The IPCE for the WO_3 photoanode in chloride oxidation solution (1 M $HClO_4$ + 3.5 M NaCl) was calculated in the same way as for the IPCE in water oxidation solution, according to equation (S8). For

example, at 300 nm, the average photocurrent density was 5.91×10^{-5} mA, which was divided by the charge of one electron (1.6×10^{-19} C), to express the photocurrent density as 3.69×10^{14} electrons s^{-1} cm^{-2}. Then, using equation (S7), and the value of photon flux for 300 nm emission determined previously (1.18×10^{15} photons s^{-1} cm^{-2}, see **Figure S5.2**), the IPCE value for the WO_3 photoanode (held at 1.3 V vs Ag/AgCl) in 1 M $HClO_4$ + 3.5 M NaCl, at 300 nm was determined as

$$\text{IPCE (1 M } HClO_4 \text{ + 3.5 M NaCl, 300 nm)} = 100 \text{ x } \frac{3.69\text{x}1014}{1.18\text{x}1015} = 31.2\ \%\ \#(S10)$$

The full IPCE spectrum obtained for the WO_3 photoanode, poised at 1.3 V vs Ag/AgCl, in 1 M $HClO_4$ + 3.5 M NaCl, is shown in red, in **Figure S5.5**, and **Figure 4** in the main text.

S6 – The PIAS/TC system

A schematic of the PIAS/TC (photoinduced absorbance spectroscopy/transient photocurrent) system used in this study is shown in **Figure S6.1**. In this system, a 150 W tungsten-halogen lamp with stabilized power supply (SLS301, Thorlabs, Newton, USA) was used as the monitoring light source. The WO_3 photoanode was irradiated with a 10 W, 365 nm LED (LZ4-44UV00-0000, LedEngin Inc., San Jose, USA), the irradiance of which was varied using a variable power supply unit (QL355P, Aim and Thurlby Thandar Instruments, Huntingdon, UK) for the LED. A diaphragm shutter (SHB1T, Thorlabs, Newton, USA), controlled by a data acquisition (DAQ) card (USB-6361, National Instruments, Austin, USA), was used to control the duration of this UVA irradiation. Two monochromators, positioned on either side of the sample, were used to set the wavelength of the monitoring light beam that was transmitted through the WO_3 photoanode. The intensity of the transmitted light was monitored using a Si photodiode detector (DET100A2, Thorlabs, Newton, USA) coupled to an amplifier (PDA200C, ThorLabs, Newton, USA) and recorded by the DAQ card. This setup allowed the change in absorbance of the WO_3 photoanode, ΔAbs, to be determined upon its irradiation by the 365 nm LED. In this work, the WO_3 photoanode was biased at a potential of 1.3 V vs Ag/AgCl, thereby allowing the photocurrent to be monitored as a function of irradiation time at the same time as that of ΔAbs.

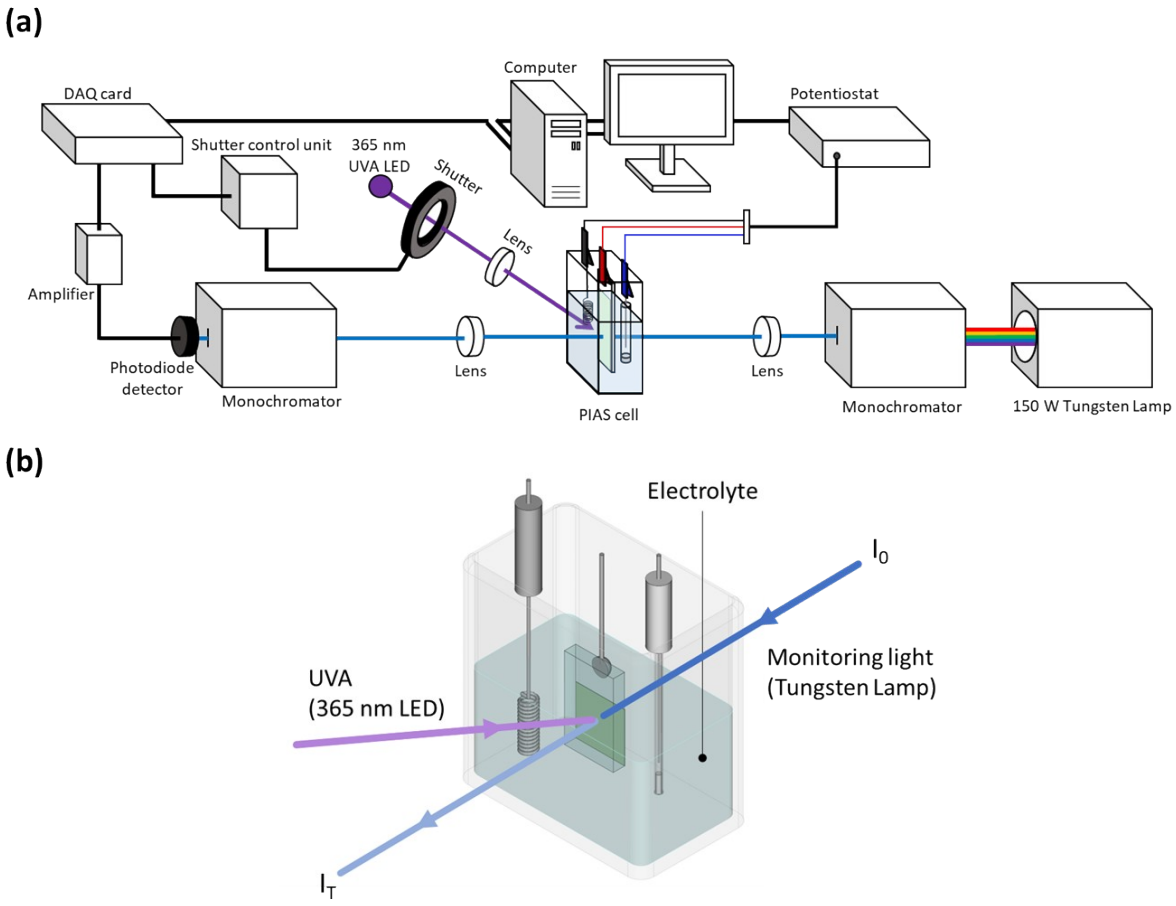

Figure S6.1 - **(a)** A schematic diagram of the setup used to obtain PIAS/TC measurements, and; **(b)** a simplified diagram of the PIAS cell showing the direction of the monitoring and excitation light, and the incident and transmitted light intensities, I_0 and I_T, respectively.

The absorbance of a sample is calculated as the $\log_{10}$ of the ratio of the incident monitoring light intensity, I_0, to its transmitted intensity after passing through the sample, I_T:

$$Abs = log_{10}\left(\frac{I_0}{I_T}\right) \#(S11)$$

In PIAS measurements, ΔAbs, the absorbance change, is calculated similarly, but instead of I_0 and I_T, the transmitted monitoring light intensity before UVA irradiation $I_{T,0}$ and the transmitted intensity at every other time, t, are used, as follows:

$$\Delta Abs = log_{10}\left(\frac{I_{T,0}}{I_{T,t}}\right) \#(S12)$$

In order to determine at which monitoring wavelength the photogenerated electron holes absorb most strongly, PIAS/TC was used to measure the ΔAbs of the WO_3 photoanode in 1 M $HClO_4$, upon 76 mW cm^{-2} 365 nm UV irradiation, using 500 nm, 600 nm, 700 nm, 800 nm and 900 nm monitoring light

wavelengths (λ_{mon} values). The resulting ΔAbs vs t profiles are shown in **Figure S6.2(a)**. ΔAbs_{ss} values were determined as the average ΔAbs values between t=7 s and t=9.5 s from these profiles, and are plotted against the λ_{mon} values under which they were obtained in **Figure S6.2(b)**, to generate a photoinduced absorbance spectrum of the WO_3 photoanode, poised at 1.3 V vs Ag/AgCl, in 1 M $HClO_4$. This spectrum reveals an absorbance maximum at 500 nm, which matches well with the previously reported absorbance maximum of photogenerated holes on WO_3 at 475 nm, obtained for a WO_3 film in a solution containing the electron scavenger $AgNO_3$,[4] (reproduced and shown in **Figure S6.2(b)**) and with other transient absorbance/diffuse reflectance studies which have reported absorbance due to photogenerated surface holes on WO_3 at 500 nm.[5, 6] If the photoinduced absorbance had been due to photo-excited electrons on WO_3, the PIAS spectrum would have been expected to show a maximum absorbance at 900-950 nm, decreasing at shorter wavelengths, in accordance with previous transient absorbance studies.[4, 5] Thus the absorbance at 500 nm was assigned to the photogenerated surface holes on the WO_3 photoanode, and 500 nm was used as λ_{mon} for the remaining PIAS/TC experiments.

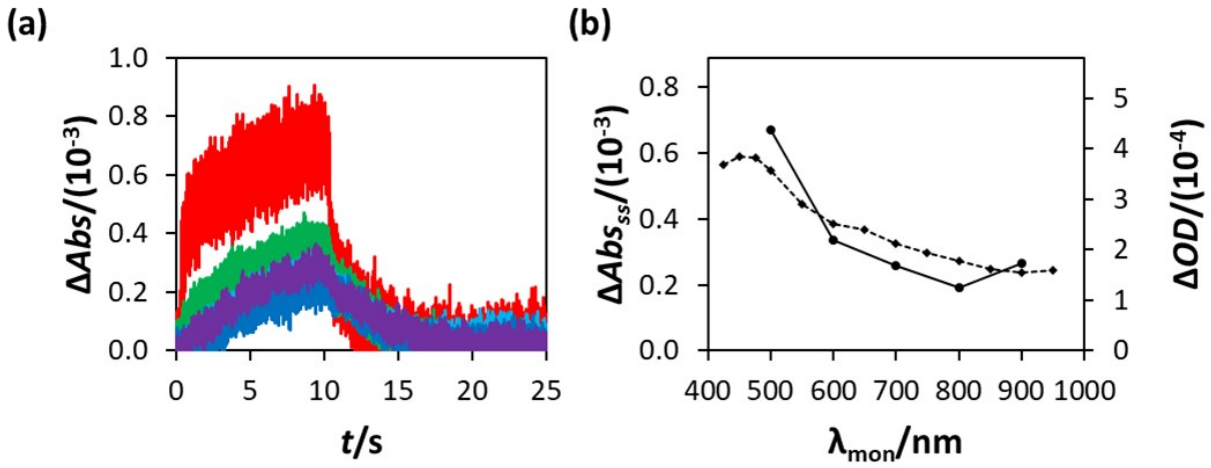

Figure S6.2 – **(a)** Photoinduced absorbance change vs t profiles for the WO_3 photoanode in 1 M $HClO_4$, poised at 1.3 V vs Ag/AgCl, irradiated with UVA light (76 mW cm^{-2}, 365 nm) between t=0 s and t=10 s, obtained using different monitoring light wavelengths: 500 nm (red), 600 nm (green), 700 nm (light blue), 800 nm (dark blue) and 900 nm (purple). **(b)** (solid line) The steady state photoinduced absorbance change (ΔAbs_{ss}) values, calculated as the average ΔAbs values between t=7 s and t=9.5 s, from (a), shown against the different monitoring light wavelength (λ_{mon}) values at which they were obtained; (dashed line) the transient absorption spectrum of a WO_3 film in electron scavenging $AgNO_3$ solution (0.01 M), 10 µs after UV excitation (355 nm, *ca*. 250 µJ cm^{-2}), reproduced from the literature.[4]

Example traces of ΔAbs (λ_{mon}=500 nm) vs t, and J vs t are shown in **Figure S6.3(a)** and **(b)** respectively. The plateau values in ΔAbs and J reached during irradiation are the steady state values of these parameters ΔAbs_{ss} and J_{ss}, calculated as the average values between t=2.5 s and t=4.5 s.

Assuming the photoinduced absorbance is due to photogenerated surface holes, h^+_s, then by Beer's law, ΔAbs_{ss} is proportional to the accumulated steady state concentration of electron holes at the

photoanode surface, [h^+_s]. If the photooxidation reaction taking place is known to be water oxidation, because f_{O2} = 1, then J_{ss}, the steady state photocurrent, is proportional to the rate of water oxidation, *R*. Therefore, it follows that the water oxidation rate law with respect to h^+_s,

$$R \propto \left[h^+{}_s\right]^n \#(S13)$$

can be expressed in terms of the experimentally measured parameters, J_{ss} and ΔAbs, as

$$J_{ss} \propto \Delta Abs^n \#(S14)$$

so that the slope of a plot of log J_{ss} vs log ΔAbs is equal to *n*, the order of water oxidation with respect to photogenerated surface electron holes.

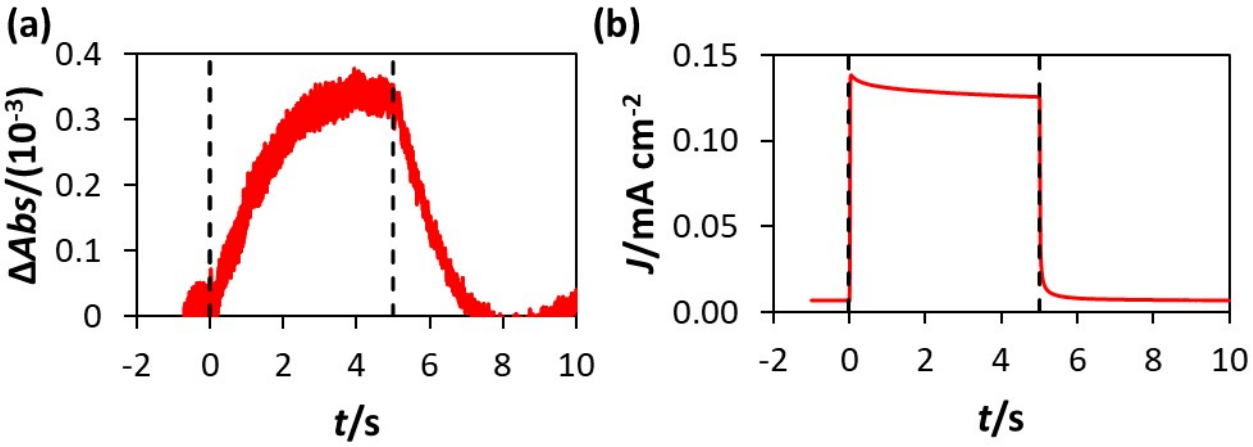

Figure S6.3 – For illustrative purposes, a typical **(a)** ΔAbs vs *t* trace and **(b)** *J* vs t trace obtained during a PIAS experiment, in which the photoanode was irradiated between t=0 s and t=5 s.

S7 – Tauc analysis of WO_3 photoanode

To determine the band gap energy of the WO_3 photoanode, a Tauc plot was generated (**Figure S7(b)**), using the measured diffuse reflectance spectrum of the WO_3 photoanode shown in **Figure S7(a)** (and in **Figure 1** in the main text). In a Tauc plot, the Kubelka-Munk converted diffuse reflectance parameter, F(R), is related to the energy of the light, hv, at each wavelength, where h is Planck's constant, and v is the light frequency (the speed of light divided by wavelength), in the form of a plot of $(F(R)hv)^{1/2}$ vs hv (the power ½ is used because the band-gap energy transition in WO_3 is indirect, if it was a direct transition, the power would be 2). Such a plot yields a linear region at higher light energies, the gradient of which intercepts the x-axis at the band-gap energy.[7] Thus, the band gap of the WO_3 photoanode used in this study was found to be 2.7 eV, consistent with the usual reported band gap values reported for WO_3 which tend to range from 2.6 – 2.8 eV.[8-11]

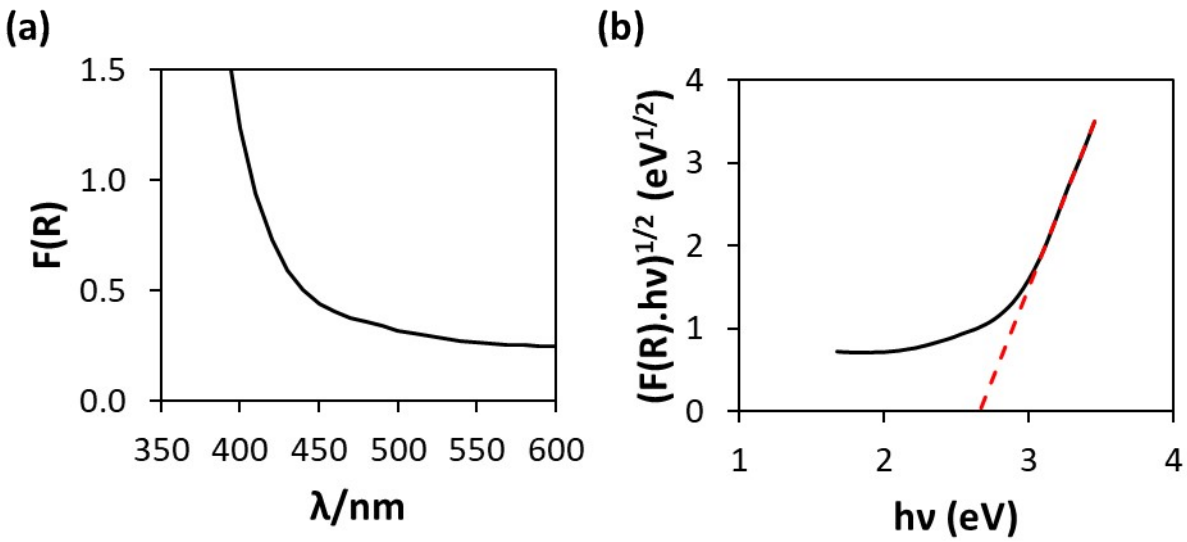

Figure S7 – **(a)** F(R) vs λ spectrum of the WO_3 photoanode where F(R) is the Kubelka-Munk remission function, determined from the diffuse reflectance (R_λ) of the photoanode ($F(R)_\lambda=(1- R_\lambda^2)/2R_\lambda$),[7] which is proportional to the ratio of the absorbance coefficient to the scattering coefficient,[12] and; **(b)** a Tauc plot showing the variation in $(F(R)hv)^{1/2}$ with hv (black), and a line of best fit for the linear portion of the plot (red), which intercepts the x-axis at the band gap energy of the WO_3 photoanode, 2.7 eV.

S8 – X-ray diffraction (XRD) pattern of WO_3 nanopowder

The X-ray diffraction (XRD) pattern of the WO_3 nanopowder used to prepare the photoanodes, and the XRD lines associated with monoclinic WO_3, shown in black and red respectively, are shown in **Figure S8**. The lines associated with monoclinic WO_3 were obtained from an international XRD database,[13, 14] and illustrate that the WO_3 used to prepare the WO_3 photoanodes in this study was monoclinic.

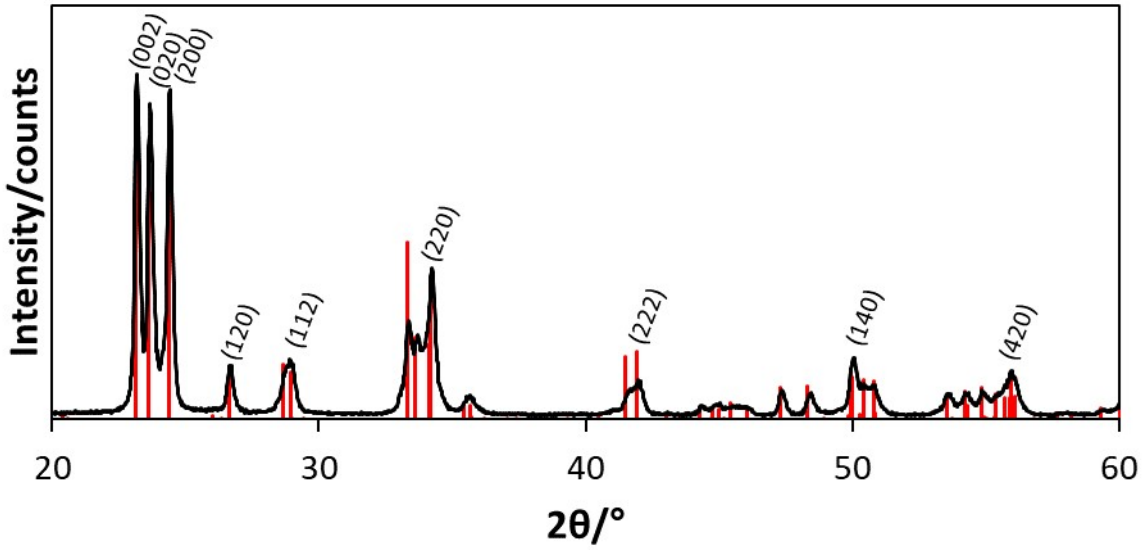

Figure S8 - X-ray diffraction pattern for the WO_3 nanopowder used to prepare the WO_3 paste photoanodes (black), with the XRD lines associated with monoclinic WO_3 (red) (obtained from an international XRD database).[13, 14]

S9 –Stability studies

In order to test the stability of the WO_3 photoanode, in $HClO_4$ and $NaCl/HClO_4$ electrolytes, each system was irradiated for 24 h using an irradiance of 40 mW cm^{-2}, with the WO_3 photoanode biased at 1.3 V (vs Ag/AgCl) applied potential, with continuous Ar purging (0.1 mL s^{-1}). The results of this work are shown in **Figure S9** and although there are some fluctuations in the traces, possibly due to surface accumulation of O_2/Cl_2 bubbles, or due to temperature fluctuations in the lab, overall both photoelectrochemical systems appeared very stable, suggesting little or no photocorrosion of the photoanode.

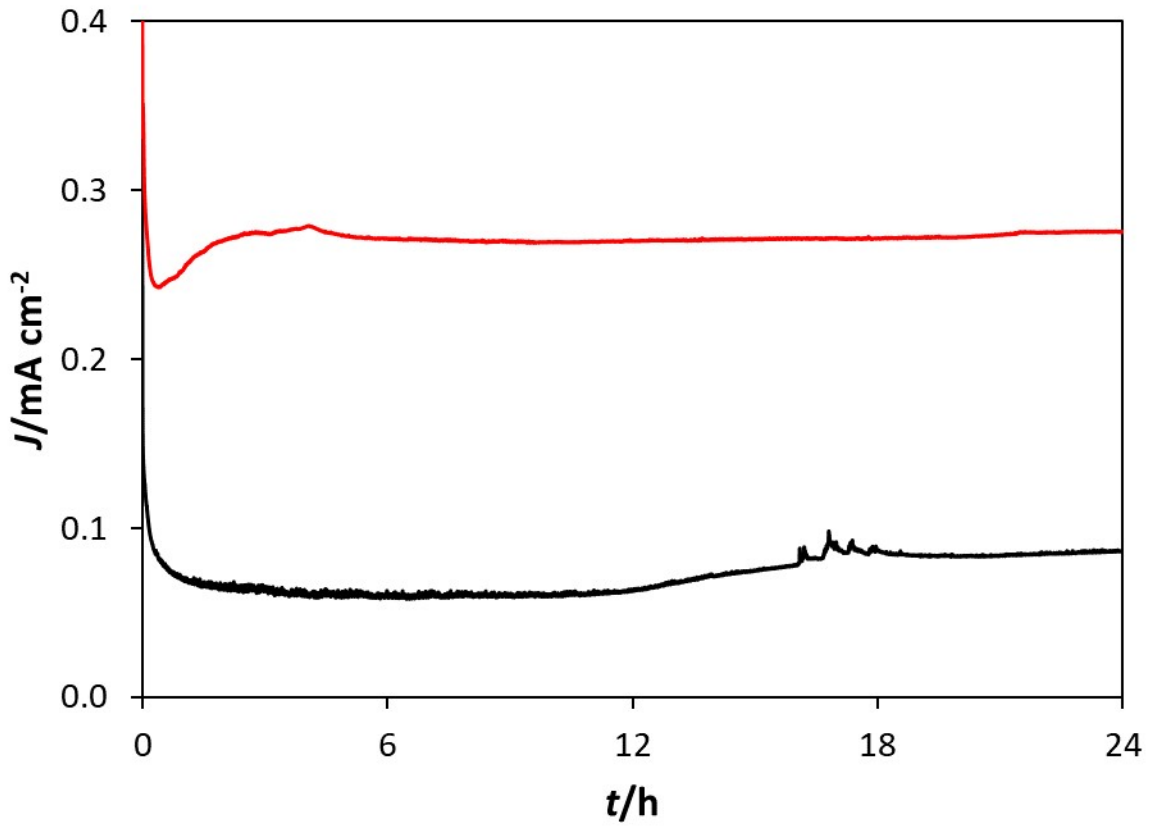

Figure S9 - Longevity study of current density, *J*, vs *t* for the WO_3 photoanode, held at 1.3 V (vs Ag/AgCl), under 40 mW cm^{-2} 365 nm UVA for 24 h, in 1 M $HClO_4$ (black trace), and in 1 M $HClO_4$ + 3.5 M NaCl (red trace), with continuous Ar purging (6 mL min^{-1}).

S10 – Detection of ClO_3^-

To account for the discrepancy in the number of electrons transferred and the amount of Cl_2 generation so that f_{Cl2}= 0.62, see **Section S3**, further work was carried out to see if chlorate, ClO_3^-, was also produced, alongside Cl_2, via the following competing oxidation reaction

$$Cl^- + 3H_2O \rightarrow ClO_3^- + 6H^+ + 6e^- \#(S15)$$

In this work, 1 mL solutions of $NaClO_3$ in 1 M $HClO_4$ + 3.5 M NaCl were prepared, where different chlorate concentrations, ranging from 0 – 1x10^{-3} M were prepared. To these 11 solutions, of different known chlorate concentration, were added 5 mL of a Lissamine green solution (1x10^{-4} M, in NaCl/$HClO_4$ electrolyte), and its decolourisation (bleaching) by the chlorate measured. The oxidation and resulting decolourisation of Lissamine green dye solution has been exploited before as a test of the oxidizing performance of a photoanode,[15] whereas here it was used to test for the presence of oxidizing agent ClO_3^- in solution.

In the above calibration work, the resulting initially orange solutions bleached over time and at a rate that was proportional to the [ClO_3^-]. Thus, after 24 h, the UV-vis spectra of the 11 solutions of known [ClO_3^-] (plus lissamine green) were obtained (**Figure S10(a)**), and for each the change in the absorbance, Δ*Abs* was determined (by subtracting the absorbance of the dye containing solution at 444 nm from that at 800 nm). The results of this calibration study were plotted in the form of Δ*Abs* vs [ClO_3^-], see **Figure S10(b)**, to reveal a linear relationship. A used electrolyte solution was then prepared, which was the residual 1 M $HClO_4$ + 3.5 M NaCl electrolyte solution following a Cl_2 yield run (30 minute irradiation (40 mW cm^{-2}, 365 nm) and applied potential (1 V vs Ag/AgCl)). When the 'used electrolyte solution' was assessed in the same way as the chlorate calibration solutions, the measured value of Δ*Abs* due to the bleaching of the Lissamine green was insignificant, suggesting little or no ClO_3^- was generated. This observation suggests that the missing 38% of oxidation product could either be $HClO_4$, or undetected Cl_2, given the highly reactive nature of the latter which could lead to a significant loss in the level of Cl_2 in the Ar gas stream as it is swept from the electrochemical reaction cell to the KI trap.

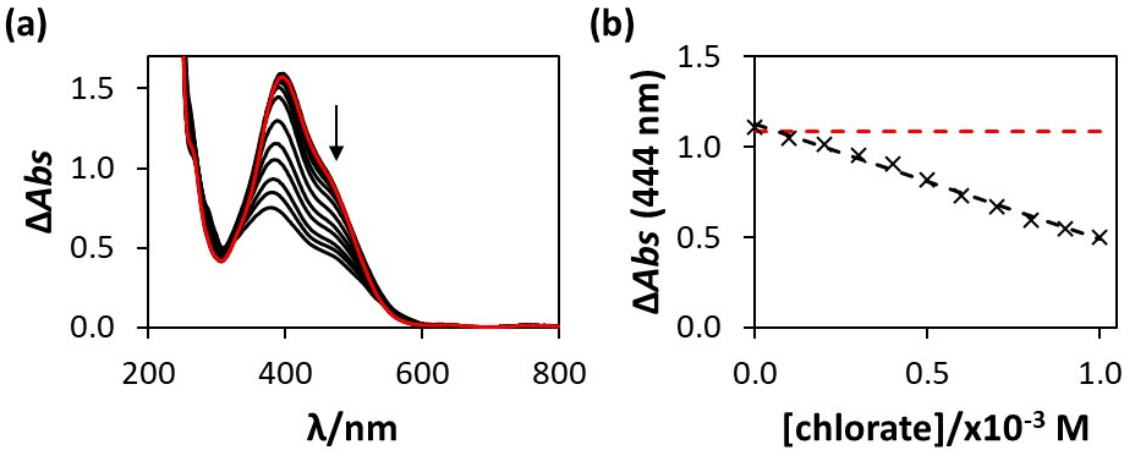

Figure S10 – **(a)** UV-vis absorbance spectra of the lissamine green test solutions with varying [ClO_3^-] (varying from 0 to 1x10^{-3} M, shown in black) and the electrolyte solution with unknown [ClO_3^-] (red), and; **(b)** the calibration plot of Δ*Abs* (444 nm) vs [ClO_3^-] (black data points and fitted trendline), and the Δ*Abs* (444 nm) of the electrolyte test solution, shown as a red dashed line.

References

1 A. Mills and A. Cook, *Analyst*, 1987, **112**, 1289-1291.

2 A. D. Awtrey and R. E. Connick, *J. Am. Chem. Soc.*, 1951, **73**, 1842-1843.

3 Z. Chen, T. F. Jaramillo, T. G. Deutsch, A. Kleiman-Shwarsctein, A. J. Forman, N. Gaillard, R. Garland, K. Takanabe, C. Heske, M. Sunkara, E. W. McFarland, K. Domen, E. L. Miller, J. A. Turner and H. N. Dinh, *J. Mater. Res.*, 2010, **25**, 3-16.

4 F. M. Pesci, A. J. Cowan, B. D. Alexander, J. R. Durrant and D. R. Klug, *J. Phys. Chem. Lett.*, 2011, **2**, 1900-1903.

5 S. Corby, E. Pastor, Y. Dong, X. Zheng, L. Francàs, M. Sachs, S. Selim, A. Kafizas, A. A. Bakulin and J. R. Durrant, *J. Phys. Chem. Lett.,* 2019, **10**, 5395-5401.

6 S. Corby, L. Francàs, S. Selim, M. Sachs, C. Blackman, A. Kafizas and J. R. Durrant, *J. Am. Chem. Soc.*, 2018, **140**, 16168-16177.

7 P. Makuła, M. Pacia and W. Macyk, *J. Phys. Chem. Lett.,* 2018, **9**, 6814-6817.

8 S. S. Kalanur, L. T. Duy and H. Seo, *Top. Catal.*, 2018, **61**, 1043-1076.

9 J. C. Hill and K.-S. Choi, *J. Phys. Chem. C*, 2012, **116**, 7612-7620.

10 M. S. Koo, X. Chen, K. Cho, T. An and W. Choi, *Environ. Sci. Technol.*, 2019, **53**, 9926-9936.

11 M. Butler, *J. Appl. Phys.*, 1977, **48**, 1914-1920.

12 K. D. Dahm and D. J. Dahm, in *Handbook of Near-Infrared Analysis*, eds. E. W. Ciurczak, B. Igne, J. Workman and D. A. Burns, CRC Press, Boca Raton, 4th edn., 2021, ch. 3, p. 33.

13 ICDD, International Centre for Diffraction Data (ICDD), https://www.icdd.com/, (accessed October 2023).

14 COD, Crystallography Open Database 1528915, http://qiserver.ugr.es/cod/1528915.html, (accessed October 2023).

15 M. K. Ensaldo-Rentería, G. Ramírez-Robledo, A. Sandoval-González, C. A. Pineda-Arellano, A. A. Álvarez-Gallegos, Á. Zamudio-Lara and S. Silva-Martínez, *J. Environ. Chem. Eng.*, 2018, **6**, 1182-1188.